Properties of Biochar Derived from Spent Mushroom Substrates

Zhuang Zhao,[a,b,†] Muhammed Mustapha Ibrahim,[a,b,c,†] Xiaodan Wang,[a,b] Shihe Xing,[a,b] Maria Heiling,[d] Rebecca Hood-Nowotny,[e] Chenxiao Tong,[a,f] and Yanling Mao [a,b,f] *

Spent mushroom substrates, *Tremella fuciformis* (Tf), *Flammulina velutipes* (Fv), and *Lentinula edodes* (Le), were used to produce biochar at different temperatures (300 °C, 400 °C, 500 °C, 600 °C, and 700 °C). Elemental compositions and surface properties of derived biochar were determined. The yield and volatile matter (VM) of the biochars decreased as the pyrolysis temperature increased with Le300 having the highest yield (47.4%). The highest VM was obtained in Tf300 (79.6%). The biochars were alkaline, with Fv700 having the highest pH (11.6). Pyrolysis temperature and feedstock influenced nutrient composition of biochars and highest values were obtained in: Tf300 (N=2.07%), Fv700 (P=12.0 g/kg), Le700 (K=21.9 g/kg), Fv600 (CEC=32.3 cmol/kg), Fv700 (Ash=33.4%) and Le700 (C=58.6%). Heavy metals in the Fv biochar were highest but within their tolerable limits. Fourier transform infrared spectra showed various functional groups on the biochar surfaces with C-O being dominant (except on Le biochar). X-ray diffraction revealed that SiO_2 and $CaCO_3$ were present on biochar surfaces. The Fv biochars had the largest surface area with Fv400 having the highest value (210.6 m^2g^{-1}) while Le400 had the highest average pore diameter (159.7 Å). These properties render the biochars suitable as soil amendment and in environmental remediation.

Keywords: Biochar; Spent mushroom substrates; pyrolysis; environmental remediation

Contact information: a: College of Resources and Environment, Fujian Agriculture and Forestry University, Fuzhou, 350002, Fujian Province, China; b: Key Research Laboratory of Soil Ecosystem Health and Regulation in Fujian Provincial University, Fuzhou, 350002, Fujian Province, China; c: Department of Soil Science, University of Agriculture, Makurdi, Nigeria; d: Soil and Water Management and Crop Nutrition Laboratory, Joint FAO/IAEA Division of Nuclear Techniques in Food and Agriculture, International Atomic Energy Agency (IAEA), Vienna, Austria; e: Department of Chemical Ecology and Ecosystem Research, University of Vienna, Vienna, Austria; f: Fujian Colleges and Universities Engineering Research Institute of Conservation and Utilization of Natural Bioresources, College of Forestry, Fujian Agriculture and Forestry University, Fuzhou, 350002, Fujian Province, China;
** Corresponding author: fafum@126.com; † Equal contribution by authors*

INTRODUCTION

Agricultural wastes, such as plant residues, are increasingly being recognized as important renewable feedstocks as a result of their carbon-rich composition (Bais-Moleman *et al.* 2018). China has a massive mushroom industry that accounts for approximately 75% of the annual global mushroom production and generates substantial amounts of spent mushroom substrate (SMS) (Mao *et al.* 2018). Gutian county of the Fujian province is one of the main production areas, which is often referred to as "the capital of Chinese edible fungus."

The total amount of SMS amounts to 30 million tons per year, and in the case of Gutian county, there were 1.02 billion bags equivalent to approximately 0.37 million tons. The current disposal strategies of SMS include burning, land spreading, burying, composting with animal manure, or landfilling (Phan and Sabaratnam 2012).

Spent mushroom substrates are used as raw materials to produce value-added products such as biogas, bulk enzymes, and organic fertilizer by bioconversion; they can also be used as animal feed supplements (Lim *et al.* 2013). Several methods of re-use have been reported, including the use as biological pesticides (Hossain *et al.* 2013), fuel and energy materials (Yadav and Samadder 2018), organic fertilizers (Paula *et al.* 2017), and other uses.

However, the authors posit that a more effective way of reusing this agricultural waste is through its conversion to biochar *via* pyrolysis. Pyrolysis is one of the most widely used thermo-chemical conversion technologies and refers to the thermal decomposition of organic components in biomass in an inert gas atmosphere with oxygen limited conditions (Kung *et al.* 2015). It produces a carbon-rich material with an abundant pore structure, which is termed biochar when it is specifically produced for soil amendment purposes (Chen *et al.* 2016).

The application of biochar has attracted increased attention because of its potential in global warming mitigation, soil fertility improvement, pollution remediation, and agricultural waste recycling. Research has shown that biochar plays an important role in improving soil structure (Song *et al.* 2018), promoting plant growth (Subedi *et al.* 2016), fixing heavy metals (Beiyuan *et al.* 2017; Wang *et al.* 2017; Yoo *et al.* 2018), reducing greenhouse gas emissions (Mechler *et al.* 2018), reducing nutrient losses (Kerré *et al.* 2017; Song *et al.* 2018), and as a carrier for bacterial inoculants (Egamberdieva *et al.* 2017, 2018).

Evident from the increasing volume of scientific literature, the use of biochar has created considerable interest in recent years. The majority of the biochar studies have concentrated on crop straws (Bian *et al.* 2018; Kang *et al.* 2018), wood (Yargicoglu *et al.* 2015; Chen *et al.* 2016; Vecstaudza *et al.* 2018; Wang *et al.* 2018), manure (Gascó *et al.* 2018; Xiao *et al.* 2018; Zhou *et al.* 2019), and municipal sludge (Wang *et al.* 2017; Kim *et al.* 2018). However, there are few, if any, comprehensive studies on the production and characterization of biochar made from different SMS and their applications based on the observed properties.

Pyrolysis temperature is the major factor that influences the properties of biochar and these properties vary depending on feedstock types (Lehmann *et al.* 2011). To address this research gap, this study was conducted to investigate the biophysical properties of three types of SMS raw materials and the derived biochar obtained through pyrolysis under different temperatures.

Nutrient composition, structure, and surface characteristics of the biochar samples were studied to obtain the most suitable uses for the derived biochar based on feedstock and pyrolysis temperature. This information will give an insight into the effective and appropriate use of these substrates, as well as providing a preliminary and theoretical basis for the application of the derived biochar into the environment.

EXPERIMENTAL

Materials

Biochar preparation

The biomass feedstocks were three types of spent mushroom substrates, *viz. Tremella fuciformis* (Tf) and *Lentinula edodes* (Le), which were collected from Gutian City, Fujian Province, China, and *Flammulina velutipes* (Fv) that was collected from the Juncao Center of Fujian Agriculture and Forestry University (Fuzhou, China). The feedstock materials were separately homogenized and broken into small pieces using a universal crusher (WN-200, Guangzhou Xulang Machinery Equipment, Guangzhou, China) to approximately 1 cm^{-3}, and subsequently air-dried for a week to reduce the moisture content to below 10%. A designed convenient biomass carbonizer (SSBP-50004, Biomass Technology Co. Ltd, Jiangsu, China.) was used for slow pyrolysis, and a constant stream of compressed nitrogen (N_2) was fed into the reactor to remove O_2 at a flow rate of 3000 NmL/min^{-1} for 2 min before the heating process began to create an oxygen-limited environment. The feedstock was fed into the carbonizer and pyrolyzed at a heating rate of 10 ℃ min^{-1} up to 300 ℃, 400 ℃, 500 ℃, 600 ℃, and 700 ℃ ± 10 ℃ for 2 h to carbonize the samples. After cooling to ambient temperature, the prepared biochar was ground using a universal crusher (WN-200, Guangzhou Xulang Machinery Equipment, Guangzhou, China) and passed through a 0.149 mm sieve for subsequent physicochemical analyses.

Methods

Feedstock and biochar characterization

Moisture and ash content of feedstock and biochar samples were determined by the ASTM E871-82 and ASTM E1755-01standards, respectively. Briefly, the moisture content of the feedstock was estimated by measuring the weight loss after drying the fresh samples at 105 °C for 24 h. Ash contents were determined by the mass loss after burning the dried samples in an open crucible in a muffle furnace for 4 h at 700 °C. To remove the effect of moisture and ash, the biochar yields were expressed into a dry ash free (*daf*) basis as follows,

$$Y_{biochar};\ daf\ (wt\%) = 100\ x\ (Y_{biochar} - A) / (100 - M - A) \quad (1)$$

$$Y_{biochar};\ ad\ (wt\%) = 100\ x\ \frac{M_{biochar}}{M_{biomass}} \quad (2)$$

where $M_{biochar}$ (wt%) represents the weight of biochar, $Y_{biochar}$; *ad* (wt%) represents the air-dried basis yields of biochar, $M_{biomass}$ represents the weight of the biomass, while *M* and *A* (wt%) are the moisture and ash contents of biomass, respectively. The volatile matter was determined by measuring the weight difference before and after the combustion of about 1 g of biochar in a crucible at 950 ºC (Li *et al.* 2018).

The pH values of samples were measured with a pH meter (PHS-3E; INESA Scientific Instrument Co., Ltd., Shanghai, China) using a 1:5, sample to deionized water (Gaskin *et al.* 2010), after stirring for 1 h at constant temperature (25 ℃). The contents of C, N, and S were determined by an elemental analyzer (VarioMax; Elementar, Lagenselbold, Germany). The P and K contents of the samples were measured using the APHA Standard Method 4500-P. Total P concentration was measured by colorimetric analysis and total K with flame atomic spectroscopy (FP640; AOPU Analytical

Instruments, Shanghai, China). The contents of heavy metals (Cd, Pb, Cr, Cu, Zn, Mn, and Ni) were measured by an inductively coupled plasma-mass spectrometer (ICP-MS) (NexlON 300X; Perkin Elmer, Waltham, MA, USA).

Cation exchange capacity (CEC) of the biochar samples was measured using the 1M ammonium acetate method (Gai *et al.* 2014). This was done by taking 0.50 g sample and leaching it with 100 mL deionized water five times to reduce the interference of soluble salts. Then, the sample was leached with 100 mL 1 mol/L^{-1} sodium acetate (pH 8.2) five times to ensure that the exchange sites were saturated with sodium ions. Thereafter, the sample was leached with 100 mL ethyl alcohol five times to remove the excess sodium ions. Finally, the sample was leached with 100 mL 1 mol $^{-1}$ ammonium acetate (pH 7) five times, and the sodium ion concentration of the reserved leachate above was measured by a flame photometer (FP640; AOPU Analytical Instruments, Shanghai, China). The cation exchange capacity (CEC) was calculated by the sodium ion concentration.

The surface areas of the samples were measured using multipoint Brunauer - Emmet -Teller (BET) (Trister II 3020; Micromeritics Instrument Corp., Shanghai, China) after degassing for 10 h at 105 ℃ to remove the substance adsorbed on the surface of biochar. The interface of the samples was observed by scanning, using an electron microscope (SEM) (Nova^{TM} NanoSEM 230; FEI Company, Hillsboro, OR, USA) with micrographs generated by topographic contrast. The samples were coated with a thin layer of gold because a conductive material was a prerequisite to generate the images. Image resolution used was high vacuum mode with magnifications of 1000, 20000, and 50000 at 1.0 nm with an acceleration voltage of 15 kV, and an energy resolution of 132 eV.

Fourier transform infrared (FTIR) spectroscopy was used to identify the chemical functional groups on the biochar sample surfaces. All the biochar samples were oven-dried at 80 °C for a period of 24 h before the FTIR analyses. Subsequently, the samples were crushed with spectroscopic grade KBr at a weight ratio of 0.5% (KBr/biochar), and then the mixture was pressed into transparent sheets. The observable FTIR spectra was obtained using a FTIR spectrometer (Nicolet iS5; Thermo Fisher Scientific, Waltham, MA, USA) scanned in the range of 400 cm^{-1} to 4,000 cm^{-1} at a resolution of 4.0 cm^{-1}.

The XRD patterns, *i.e.*, mineralogical characterization of the biochar samples were obtained using an X-ray diffractometer (Ultima IV; Rigaku Corporation, Wilmington, MA, USA). The samples were scanned in the range of 5° to 85° at 40 kV and 40 mA and at a speed of 6° min^{-1}. Jade 6.0 software (Jade Software Corporation, Christchurch, New Zealand) was used to remove the background radiation of the XRD results.

Data processing and statistical analysis

Collected data was subjected to analysis of variance (ANOVA) using SPSS 20.0 software (IBM Corp, Armonk, NY, USA). The means were separated using the least significant difference (LSD) at a 5% level of probability ($P < 0.05$). Origin 9.0 (OriginLab, Northampton, MA, USA) and Jade 6.0 software (Jade Software Corporation, Christchurch, New Zealand) were used to process the figures for FTIR and XRD, respectively.

RESULTS AND DISCUSSION

Physicochemical Properties of Feedstock Biomass and Biochar

The physicochemical properties of the feedstock biomass and biochar samples are shown in Tables 1 and 3, respectively. As shown in Table 1, feedstock compositions had lower values compared to the derived biochar as previously reported (Bian *et al.* 2018; Wang *et al.* 2018). The results in Table 3 show that the biochar yield decreased with increased pyrolysis temperature as earlier reported (Zhang *et al.* 2015; Gascó *et al.* 2018). Temperature is known to be the major factor influencing biochar mass yield (Weber and Quicker 2018). In addition, the rate of weakening and disappearance of peaks of functional groups present on the biochar surfaces at higher temperature such as –OH and C-H groups is consistent with a significant mass loss (Jin *et al.* 2016). All of the biochar had the highest yields at 300 ℃. The Le had a relatively high production yield compared to the other feedstocks with a peak value of 47.4% at 300 ℃. The Fv biochar had the least yield ranging from 33.7% at 300 ℃ to 30.3% at 700 ℃. The C=C stretching vibrations identified in the Tf and Le biochars produced at low temperatures 300 °C could be one of the factors that increased its initial resistance to degradation resulting to higher yields at this temperature compared to the Fv biochars. An early stabilization of yield was observed in the Tf and Fv biochar where the yield ranged from 41.0% to 38.6% and from 33.7% to 30.3%, respectively, from 300 ℃ to 700 ℃. The stabilization of biochar yield suggested that the major carbonization was completed between this temperature range. Dunnigan *et al.* (2018) observed higher yields between 400 ℃ and 550 ℃ using rice husk as feedstock. Contrary to this trend, stabilization of yield was observed at elevated temperatures of 600 ℃ to 800 ℃ using switch-grass, water oak, biosolid (Li and Chen 2018), and agricultural residues (Jindo *et al.* 2014). The variation in yield with respect to the biochar could have been a result of the different feedstocks used. The decrease in yield of biochar with increasing temperature as observed in this study has also been reported using Rhodes grass and palm fronds (Jouiad *et al.* 2015), cellulosic and lignocellulosic biomass (Peng *et al.* 2011; Hmid *et al.* 2014), and animal manures (Cely *et al.* 2015). Biochar yield decline may have been attributed to the primary decomposition of the biomass and a possible secondary decomposition of the produced biochar during the pyrolysis process at higher temperatures. The decrease in yield of biochar with increasing pyrolysis temperature was attributed to increased gasification (Colantoni *et al.* 2016). At a high pyrolysis temperature, there is an intensified carbonization of the biomass through rapid dehydrogenation, gasification, and condensation, resulting in the reduction of solid biochar produced (Li and Chen 2018). Generally, more organic matter decomposes as the temperature increases, thereby resulting in the feedstock materials with lower yields at higher pyrolysis temperatures (Ghanim *et al.* 2016; Li *et al.* 2016).

The ash content of the biochar gradually increased with the increasing temperature. Ash content was found to range from 20.6% in Le biochar at 300 ℃ to 33.4% in Fv biochar at 700 ℃, indicating that the highest ash content was derived at 700 ℃ in the Fv biochar. Although higher ash contents were observed at 500 ℃ and 600 ℃ in the Tf and Le biochar, suggesting that other factors apart from temperature could also affect the ash composition of biochar. Ash content of biochar has been previously reported to increase with rising pyrolysis temperature, and it varied among different biochar depending on the type of feedstock (Cely *et al.* 2015; Bian *et al.* 2016). The biochar had variable ash contents,

suggesting the ash composition was influenced by the nature of feedstocks. Xiao *et al.* (2018) also reported that ash contents along with specific inorganic compositions in the biochar generally increased with rising pyrolysis temperature. A positive correlation was observed between the biochar yield and both the feedstock and biochar ash content (Windeatt *et al.* 2014).

Among the feedstocks investigated, Tf had the highest volatile matter (VM) content (84.2%), followed by Fv (80.0%) and Le (72.0%) (Table 1). A decrease in VM content in biochar as pyrolysis temperature increased was observed in the biochars (Table 3). Such decrease in VM with temperature has been reported by Li *et al.* (2018) on switch grass, water oak, and biosolids. This was attributed to the fact that more VM was removed while ash and fixed carbon were retained at higher pyrolysis temperatures (Cantrell *et al.* 2012). However, the Le biochar had a lower VM compared to Tf and Fv, which may have resulted to its higher yield observed in Le300. The high amount of VM content of the biochars at lower temperatures could be due to the presence of cellulose and hemicellulose (Jindo *et al.* 2014). There was no significant difference in the VM content at 600 °C and 700 °C suggesting that majority of the VM could have been decomposed at 600 °C. Subsequently, at temperatures above 600 °C, no significant decrease in VM was observed, as also reported by Li *et al.* (2018).

Table 1. Physicochemical Properties of Feedstock Biomass

Sample	pH	Moisture Content (%)	Ash (%)	Volatile Matter (%)	C (%)	N (%)	S (%)	C/N	Total P (g kg^{-1})	Total K (g kg^{-1})
Tf	6.12 ± 0.03a	2.38 ± 0.04b	9.68 ± 0.09a	84.22 ± 1.01a	40.00 ± 2.36b	2.05 ± 0.03a	1.60 ± 0.04a	19.51 ± 1.69c	2.80 ± 0.21b	3.79 ± 0.31b
Fv	5.83 ± 0.04b	4.76 ± 0.10a	8.24 ± 0.12b	79.95 ± 0.72b	41.24 ± 1.06a	1.38 ± 0.04b	0.7 ± 0.05b	29.88 ± 2.34b	4.17 ± 0.36a	2.43 ± 0.24c
Le	4.18 ± 0.03c	2.38 ± 0.02b	9.40 ± 0.07a	71.99 ± 0.44c	39.52 ± 3.06b	1.12 ± 0.05b	0.91 ± 0.03b	35.29 ± 3.05a	2.53 ± 0.25c	10.13 ± 0.65a

Means with similar letters are statistically similar. Those with different letters are significantly different ($P < 0.05$)

As shown in Table 1, the pH values of the feedstock ranged between 4.2 to 6.1, indicating that they were strongly to moderately acidic, with Le possessing the statistically lowest pH. However, pH of the all the biochar samples ranged from 8.2 to 11.6 (Table 3). Alkaline properties of biochar have previously been reported (Cely *et al.* 2015; Mechler *et al.* 2018). Differences in pH were observed for the different biomass types. However, the Tf biochar had higher pH values across the various temperatures than other biochar produced at similar pyrolysis conditions, and the data showed that pH values increased as the temperature increased, indicating that the pyrolysis temperature had a profound effect on the pH of the derived biochar.

Table 2. Heavy Metal Contents of Feedstock Biomass

Sample	Unit: mg kg^{-1}						
	Cr	Mn	Ni	Cu	Zn	Cd	Pb
Tf	33.58 ± 2.36a	113.06 ± 5.62c	7.59 ± 0.28c	15.32 ± 1.03b	208.85 ± 10.36b	0.11 ± 0.03c	5.29 ± 0.17c
Fv	25.66 ± 2.06b	300.53 ± 4.31b	14.01 ± 0.91a	20.87 ± 1.52a	281.94 ± 7.02a	0.41 ± 0.04a	26.45 ± 2.43a
Le	26.35 ± 1.67b	356.14 ± 6.94a	10.98 ± 0.51b	16.94 ± 2.31b	120.81 ± 5.36c	0.15 ± 0.02b	9.44 ± 1.05b

Means with similar letters are statistically similar. Those with different letters are significantly different ($P < 0.05$)

Table 3. Physicochemical Properties of Biochar

Sample	Yield (%)	pH	Ash (%)	Volatile Matter (%)	CEC (cmol kg^{-1})	C (%)	N (%)	S (%)	C/N	Total P (g kg^{-1})	Total K (g kg^{-1})
Tf300	40.98 ± 1.36a	11.32 ± 0.09c	27.48 ± 0.85b	79.57 ± 0.42a	28.53 ± 0.35ab	53.49 ± 2.36ab	2.07 ± 0.06a	0.14 ± 0.02a	25.89 ± 1.66c	7.12 ± 0.21a	13.37 ± 0.65b
Tf400	40.25 ± 2.03b	11.34 ± 0.12c	26.92 ± 0.65bc	77.14 ± 0.55b	28.98 ± 0.61a	54.19 ± 1.36a	2.04 ± 0.05a	0.12 ± 0.03a	26.61 ± 1.53bc	7.21 ± 0.36a	12.41 ± 0.54c
Tf500	40.25 ± 1.65b	11.36 ± 0.06c	28.04 ± 0.76a	77.05 ± 0.72b	26.73 ± 1.57b	54.32 ± 3.25a	2.00 ± 0.04a	0.12 ± 0.01a	27.19 ± 0.96b	7.03 ± 0.16b	15.12 ± 0.40a
Tf600	39.89 ± 0.96c	11.46 ± 0.11b	26.48 ± 0.36c	69.11 ± 0.47c	28.95 ± 0.62a	52.99 ± 2.67b	1.90 ± 0.07b	0.11 ± 0.01a	27.92 ± 2.05b	6.57 ± 0.13c	14.53 ± 0.13a
Tf700	38.62 ± 1.36c	11.63 ± 0.06a	26.64 ± 1.02c	68.97 ± 0.84c	26.71 ± 0.73b	52.6 ± 2.04b	1.80 ± 0.06c	0.07 ± 0.04b	29.30 ± 1.62a	7.00 ± 0.42b	13.34 ± 0.45b
Fv300	33.67 ± 0.91a	9.84 ± 0.14c	25.82 ± 0.91c	69.04 ± 0.77a	28.96 ± 0.75c	56.61 ± 3.57b	1.67 ± 0.04a	1.49 ± 0.06b	33.9 ± 0.98c	11.07 ± 0.4d	8.65 ± 0.54b
Fv400	33.11 ± 1.36a	10.02 ± 0.08c	25.84 ± 0.42c	66.90 ± 0.63b	30.84 ± 0.91b	56.83 ± 3.14ab	1.63 ± 0.07a	1.60 ± 0.07a	34.87 ± 1.36c	11.16 ± 0.30c	8.89 ± 0.61b
Fv500	31.75 ± 2.15b	10.84 ± 0.16b	27.57 ± 0.35b	64.71 ± 1.07c	30.12 ± 0.35bc	58.61 ± 2.05a	1.57 ± 0.06ab	1.34 ± 0.1c	37.33 ± 1.12b	11.22 ± 0.17c	8.29 ± 0.16c

Fv600	31.71 ± 1.61b	10.77 ± 0.14b	24.92 ± 0.62c	60.44 ± 0.98c	32.29 ± 0.43a	57.31 ± 1.65a	1.48 ± 0.12b	1.32 ± 0.06c	38.67 ± 2.60b	11.46 ± 0.32b	9.91 ± 0.36a
Fv700	30.31 ± 2.16c	11.64 ± 0.05a	33.40 ± 0.71a	59.36 ± 0.69c	25.71 ± 0.54d	54.85 ± 2.63c	1.16 ± 0.06c	1.32 ± 0.07c	47.44 ± 2.25a	11.95 ± 0.24a	9.73 ± 0.14a
Le300	47.41 ± 0.75a	8.23 ± 0.06d	20.62 ± 0.16d	62.45 ± 0.79a	27.15 ± 0.51a	53.6 ± 3.51c	1.42 ± 0.06a	0.49 ± 0.05a	37.86 ± 2.64c	2.88 ± 0.23c	10.73 ± 0.06c
Le400	38.00 ± 1.81b	9.92 ± 0.14c	25.62 ± 0.66c	60.21 ± 0.65b	26.29 ± 0.15a	54.11 ± 2.54c	1.41 ± 0.08ab	0.21 ± 0.01b	38.45 ± 1.9bc	2.90 ± 0.13c	15.12 ± 0.37b
Le500	32.78 ± 0.61c	10.24 ± 0.07b	28.52 ± 0.64b	57.59 ± 0.49c	20.00 ± 0.21c	54.97 ± 2.69bc	1.34 ± 0.07b	0.12 ± 0.03c	40.99 ± 3.04b	4.11 ± 0.14b	16.33 ± 0.07b
Le600	31.6 ± 1.57c	10.53 ± 0.13ab	31.62 ± 0.51a	55.17 ± 0.73d	23.61 ± 0.64b	55.84 ± 1.4b	1.19 ± 0.09c	0.04 ± 0.04d	46.76 ± 2.05a	5.62 ± 0.32a	17.76 ± 0.13b
Le700	31.9 ± 2.07c	10.69 ± 0.05a	28.28 ± 0.25b	54.14 ± 0.88d	19.37 ± 0.4c	58.65 ± 3.25a	1.5 ± 0.12a	0.06 ± 0.02d	39.13 ± 2.68b	5.01 ± 0.11a	21.89 ± 0.67a

Means with similar letters are statistically similar. Those with different letters are significantly different ($P < 0.05$) for individual biochar

The highest pH was recorded at 700 ℃ in the Fv biochar. Generally, high pH values are a result of an accumulation of high alkali metals (Ca, Mg, K, and Na) due to the thermal degradation of the organic fraction in biomass during the pyrolysis process (Kim *et al.* 2018). In addition, at higher pyrolysis temperatures, the amount of carboxyl groups in the resulting biochar are reduced and/or the acidic groups have become deprotonated to the conjugate bases, resulting in a more alkaline pH of the biochar in suspension (Ronsse *et al.* 2013). The rise in pH at higher pyrolysis conditions could also be attributed to the relative increase in ash content in the biochar. Biochar produced at higher pyrolysis temperatures are therefore expected to have more advantages in agriculture as they can improve of soil health because the alkalinity of biochar (Molnar *et al.* 2016) which could create a preferable environment for the soil microbial communities that function in C and N cycling (Jaafar *et al.* 2015). Therefore, pyrolysis temperature, nature and composition of feedstock can be determining factors to produce biochar with specific uses such as soil amendment.

Elemental composition analysis of feedstock biomass and derived biochar samples indicated that biomasses were typically lower in nutrient composition compared to the derived biochar (Tables 1 and 3). Pyrolysis temperatures had large impacts on the biochar's elemental composition during the pyrolysis process. One main goal of biochar production is the change in chemical composition compared to that of raw biomass, more importantly the increase in carbon content (Weber and Quicker 2018). In general, when the temperature rose from 300 °C to the peak temperature of 700 ℃, carbon contents initially increased and subsequently decreased at 600 ℃ for all of the feedstocks except Le, where there was a uniform increase with increasing temperature. The highest C content was observed at 500 °C for Fv and Tf biochar, with Fv having the higher value of 58.61% (Table 3). The C contents in the biochar samples were in the range of values obtained using other feedstocks in previous reports (Sun *et al.* 2014; Chen *et al.* 2016). However, Case *et al.* (2015) reported C content of 72.3% in biochar derived from hardwood trees as feedstock at 400 ℃. This suggests that feedstock materials determine the C composition of derived biochar. The sharp decline of C contents in all the biochar at the peak temperature of 700 ℃ could be attributed to the loss of C-containing compounds during pyrolysis at elevated temperatures (Han *et al.* 2016; Wang *et al.* 2016). Similar temperature effects on carbon contents have previously been observed (Bergeron *et al.* 2013). The relatively high C content of these biochar makes them suitable for C sequestration of excess carbon from the atmosphere (Herath *et al.* 2015).

Nitrogen content decreased as pyrolysis temperature increased across all the biochars evaluated. However, there was an observed increase in the N content of Le biochar from 600 ℃ to 700 ℃. The Tf biochar contained relatively higher N contents (1.80% to 2.07%) compared to the others and could be of greater benefit when used as N fertilizer. Although compared to its feedstock that contained 2.05% N, the Tf biochar contained its highest N content of 2.07% at 300 ℃. However, N content in biochar derived from 400 ℃ to 700 ℃ (Table 3) for the Tf biochar were lower than that of the feedstock (Table 1), suggesting that the Tf biochar had a high quantity of volatile N-containing compounds that volatilized at higher pyrolysis temperatures. The nature of the feedstock material also had an influence on the N content, as the Le biochar made from hardwood feedstock had a lower N content. The highest N content was obtained at 300 ℃, indicating that the pyrolysis temperature had a significant effect on the N contents. The decrease in biochar N content was probably due to volatilization of N-containing compounds associated with the decomposition of amino acids as the temperature increased (Xiao *et al.* 2018). Therefore, the ratio of C:N increased in all of the biochar samples except for Le biochar at 700 ℃.

Similarly, sulfur contents decreased with increasing temperature, but this was not consistent across all the biochar as the Fv400 increased to 1.60 % from 1.49 % in Fv300 before declining. The observed decrease in sulfur may be due to the decomposition of organic sulfur during pyrolysis (Nanda *et al.* 2014). There was an increase in potassium and phosphorus contents as the pyrolysis temperature increased, although an irregular pattern emerged. Increase in these elements with an increase in pyrolytic temperature has also been observed (Ahmad *et al.* 2017). Such increases in these non-volatile elements have been previously reported (Colantoni *et al.* 2016). There were no clear trends of cation exchange capacity (CEC) with increasing temperature, but values declined at the peak temperature of 700 °C, with Fv600 having the highest CEC (32.29 cmol kg^{-1}). The higher CEC value of this biochar indicated its stronger ability to hold essential nutrients as well as greater its resistance against soil acidification (Mukherjee *et al.* 2011). A similar observation was made using switchgrass, water oak, and biosolids where CEC declined at the peak temperature of 800 °C (Li and Chen 2018). The CEC is a measure of the ability of materials to adsorb cations such as Ca^{2+}, Mg^{2+}, or K^{+}. Gascó *et al.* (2018) used pig manure feedstocks and observed the highest CEC values at 600 °C.

Table 4. Heavy Metal Contents of Biochar

Sample	Cr (mg kg^{-1})	Mn (mg kg^{-1})	Ni (mg kg^{-1})	Cu (mg kg^{-1})	Zn (mg kg^{-1})	Cd (mg kg^{-1})	Pb (mg kg^{-1})
Tf300	61.85 ± 3.49a	243.47 ± 12.36b	9.80 ± 1.36c	24.21 ± 2.36b	261.79 ± 2.36b	0.35 ± 0.04a	11.54 ± 0.93a
Tf400	44.84 ± 2.64c	234.40 ± 9.64c	9.66 ± 0.96bc	22.41 ± 1.39b	317.2 ± 5.36a	0.21 ± 0.06c	10.67 ± 0.61b
Tf500	51.33 ± 1.34b	240.59 ± 13.64b	13.34 ± 1.12a	29.86 ± 1.68a	237.59 ± 3.35c	0.19 ± 0.06c	9.10 ± 1.06c
Tf600	58.57 ± 2.49a	260.12 ± 8.65a	12.28 ± 1.32a	29.60 ± 0.68a	239.38 ± 2.39c	0.27 ± 0.01b	8.26 ± 0.64d
Tf700	47.17 ± 2.68c	241.12 ± 10.36b	10.71 ± 0.68b	29.23 ± 0.94a	274.16 ± 4.66b	0.38 ± 0.05a	12.03 ± 0.61a
Fv300	57.19 ± 2.16b	808.50 ± 6.36b	36.41 ± 0.94a	45.00 ± 1.76a	432.84 ± 3.69a	0.56 ± 0.02b	57.40 ± 2.61b
Fv400	58.34 ± 2.61b	783.16 ± 5.36c	38.29 ± 1.17a	39.95 ± 2.91c	353.02 ± 1.36c	0.6 ± 0.04b	58.88 ± 3.16b
Fv500	53.53 ± 3.46c	734.96 ± 10.61c	33.79 ± 3.05b	39.47 ± 1.36c	409.2 ± 2.95b	0.78 ± 0.04a	59.47 ± 0.69b
Fv600	56.08 ± 2.66b	814.78 ± 6.36b	35.13 ± 2.17ab	43.66 ± 0.61a	336.17 ± 6.46d	0.40 ± 0.06c	63.04 ± 1.13a
Fv700	69.70 ± 1.34a	1121.47 ± 12.36a	22.03 ± 1.68c	41.72 ± 2.35b	341.16 ± 5.37cd	0.26 ± 0.06d	49.17 ± 1.69c
Le300	42.36 ± 1.34c	380.84 ± 5.36b	17.24 ± 0.94d	30.73 ± 1.21c	173.32 ± 2.36c	0.45 ± 0.12a	14.00 ± 1.36c
Le400	53.65 ± 3.05b	393.93 ± 2.16b	29.89 ± 1.31c	40.30 ± 1.65b	186.85 ± 5.10c	0.49 ± 0.05a	20.42 ± 2.31b
Le500	56.36 ± 3.65b	413.52 ± 6.38a	25.61 ± 2.36c	39.86 ± 0.45b	230.48 ± 3.69b	0.23 ± 0.08b	20.09 ± 1.70b
Le600	64.86 ± 2.61a	372.43 ± 8.62c	51.44 ± 0.91a	46.83 ± 2.36a	243.10 ± 4.16a	0.39 ± 0.05a	8.88 ± 1.60c
Le700	62.69 ± 1.68a	380.36 ± 10.36b	36.09 ± 3.66b	45.91 ± 1.82a	244.18 ± 2.65a	0.04 ± 0.03d	24.04 ± 1.16a

Moreover, Cely *et al.* (2015) showed that the CEC of biochar depends on the pyrolysis temperature and raw material properties. The greater CEC of the biochar could have been a result of a higher charge density per unit surface area, the formation of carboxyl groups, a more porous structure, or a combined effect of the three factors (Sun *et al.* 2014). Therefore, the biochars produced at 600 ℃ and below will be of greater advantage as soil amendments in agronomy based on the CEC. Generally, the biochar materials used herein were generally high in nutrient composition compared to their feedstock materials. These properties render the derived biochar of high agronomic value (Wang *et al.* 2015; Domingues *et al.* 2017) and can thus be used as soil amendments, especially in combination with organic and inorganic fertilizers. But this factor was outside the scope of this study and such research is suggested to be undertaken.

As can be seen in Table 4, the biochar generated from 500 ℃ to 600 °C contained higher concentrations of metals as compared to those produced at 300 °C and 400 ℃. Higher pyrolysis temperatures resulted in biochar with higher micronutrients content. Kim *et al.* (2018) observed a similar trend using sludge, rice straw, and spent coffee ground biochar from 550 °C and 700 °C and attributed this phenomenon to the higher degree of thermal degradation of the organic mass faction in samples pyrolyzed at a higher temperature. The Zn content did not follow this trend in the Fv biochar, as the highest value of 432.8 mg kg^{-1} was observed at 300 °C. There was also an irregular effect of pyrolysis temperature on the Cd and Pb contents in all of the biochar. The Ni content was drastically reduced at the peak temperature of 700 °C in all the biochar samples. This may have been attributed to Ni containing compounds being degraded at relatively high temperatures. Generally, the highest concentration of heavy metals was obtained in the Fv feedstock and derived biochar (Tables 2 and 4). This illustrated its importance of the immobilization of heavy metals and can be a useful trait in bioremediation. Detoxification of heavy metal ions, to variable extents, can be achieved by introducing biochar into the soil as they can form specific complexes with these metals (Han *et al.* 2013). It has been demonstrated that biochar has an excellent ability to immobilize metals and organic contaminants from the aqueous phase and soil (Beiyuan *et al.* 2017; Wang *et al.* 2017; Yoo *et al.* 2018). However, the bioavailability of these metals in the biochar should be further studied to ensure their safe use. The EBC (2017) gave the acceptable range of heavy metals in biochar on a dry matter basis as stated: Pb < 150 mg kg^{-1}; Cd < 1.5 mg kg^{-1}; Cu < 100 mg kg^{-1}; Ni < 50 mg kg^{-1}; Zn < 400 mg kg^{-1} and Cr < 90 mg kg^{-1}. The results (Table 4) show that all the heavy metals in the obtained biochar were within safe limits except Zn, which was a bit higher than the threshold given for the metal in biochar in the Fv biochar as well as Ni in Le600 biochar. Zinc content ranged from 173.32 mg kg^{-1} at 300 °C in the Le biochar to 432.84 mg kg^{-1} at 300 °C in the Fv biochar. The content of Ni in Le600 was 51.44 mg kg^{-1} which was above the threshold of 50 mg kg^{-1} given. However, this does not call for serious concern as the amounts of biochar used in agriculture are relatively low compared to those of compost and manure. Therefore, toxic accumulation of heavy metals could practically be ruled out, even when thresholds are higher (EBC 2017) and as such, these biochar materials could be useful soil amendments without any environmental concern.

Microstructure and Surface Functional Analysis of Biochar

The SEM images of biochar taken under different magnification times at 400 ºC to investigate their surface structures are shown in Figs. 3 to 5. It was obvious from the images that the surface morphology of the biochars varied and can be largely attributed to the

nature of feedstocks. As shown on Fig. 5, SEM images of the Le400 biochar even at a lower magnification time (x20000) compared to Tf400 and Fv400 (x50000) in Figs. 3 and 4 respectively showed higher pores and relatively lower surface area as also reported on Table 5 and Fig. 1. The images also indicated the presence of porous structure on the surfaces, but Fig. 3 and 4 showed that some pores were filled by volatile matter, which decreased the average pore diameter (Table 5 and Fig. 1). The presence of volatiles in the pore structure of biochar on SEM images has been reported in rice husk and elm sawdust biochar (Wang *et al.* 2014).

The pore distribution (Table 5, Fig 1) revealed a porous structure of all the biochar, with little variation between the biomass feedstock types, except for the Le biochar that showed higher average pore diameter ranging from 37.6 Å at 600 ℃ to 159.7 Å at 400 ℃ (Fig 1).

Table 5. BET Surface Area and Porosity of Biochar

Sample	BET Surface Area (m^2 g^{-1})	t-plot Micropore Area (m^2 g^{-1})	t-plot Micropore Volume (cm^3 g^{-1})	Adsorption Average Pore Diameter (Å)
Tf300	49.58 ± 2.61a	32.63 ± 2.06b	0.0169 ± 0.00115ab	33.78 ± 2.40c
Tf400	42.03 ± 1.36b	32.37 ± 3.06b	0.01675 ± 0.00205b	37.1 ± 3.06a
Tf500	51.73 ± 2.61a	34.02 ± 2.61a	0.01758 ± 0.0016a	35.07 ± 2.16b
Tf600	24.47 ± 1.66d	27.66 ± 1.61d	0.01407 ± 0.00096c	37.40 ± 1.60a
Tf700	36.53 ± 2.06c	30.95 ± 3.61c	0.01598 ± 0.00065b	35.80 ± 3.16b
Fv300	156.78 ± 4.26c	133.41 ± 2.61c	0.06901 ± 0.00354bc	24.81 ± 1.40b
Fv400	210.57 ± 2.36a	175.07 ± 2.30a	0.09042 ± 0.0016a	25.64 ± 1.65b
Fv500	175.46 ± 6.06b	144.98 ± 5.15b	0.07502 ± 0.00155b	25.92 ± 3.45b
Fv600	148.30 ± 1.60c	110.5 ± 2.39d	0.05706 ± 0.0030c	30.41 ± 2.05a
Fv700	176.62 ± 2.4b	136.93 ± 3.66c	0.07072 ± 0.0045b	25.80 ± 3.56b
Le300	3.95 ± 0.43c	5.85 ± 2.16c	-	83.80 ± 2.25b
Le400	3.09 ± 0.61c	1.88 ± 1.61c	0.00060 ± 0.00005c	159.69 ± 2.15a
Le500	5.71 ± 0.35c	3.22 ± 2.36c	0.00170 ± 0.00016c	153.37 ± 1.50a
Le600	73.56 ± 2.04a	50.32 ± 3.16a	0.02600 ± 0.0026a	37.60 ± 1.62d
Le700	21.75 ± 1.03b	14.28 ± 2.64b	0.00740 ± 0.00006b	64.28 ± 1.79c

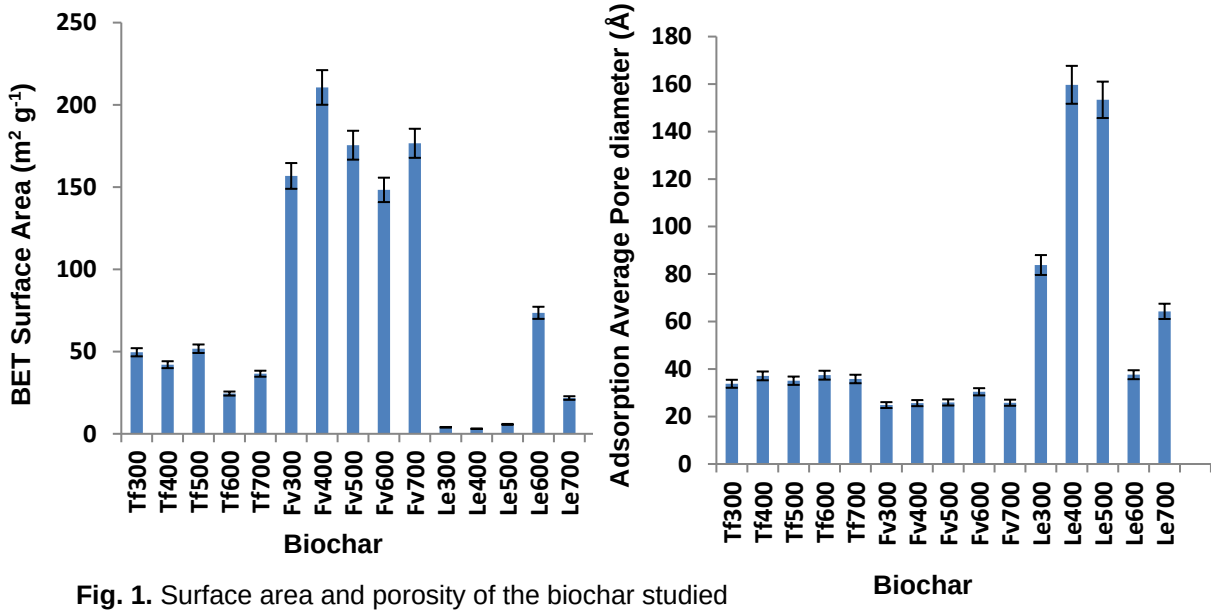

Fig. 1. Surface area and porosity of the biochar studied

The highest pore diameter of 159.69 Å was observed in the Le biochar at 400 ℃ and was drastically reduced at higher temperatures (600 ℃ to 700 ℃). This could have been attributed to the nature of the feedstock, as thermal decomposition of the raw biomass did not fully occur until higher temperatures. The higher average pore diameter of this biochar at 400 ℃ and 500 ℃ will result to a smaller surface area and might limit the adsorption capacity of this biochar in the soil. The Tf and Fv biochar had their highest pore diameter at 600 ℃. During pyrolysis, there is an increase in porosity of the resulting biochar due to the release of volatiles and chemical reactions that occur between the volatiles, minerals, and inorganic compounds that exist in the biomass (Bian *et al.* 2016). The BET surface area of the biochar samples in this study ranged from 3.09 $m^2 g^{-1}$ in the Le biochar at 400 ℃ to 210.57 $m^2 g^{-1}$ in the Fv biochar at 400 ℃ (Table 5 and Fig 1).

There was no specific effect of temperature on the surface area as there was an irregular pattern observed across the biochar types. However, the surface area was dependent on the nature of feedstock because at the same temperatures with other feedstocks, Fv biochar had higher surface areas. Although, lower surface areas at low temperatures using pine wood, wheat straw, green waste, and dried alga has been observed (Ronsse *et al.* 2013). When the pyrolysis temperature was further increased, the BET surface area either reduced or decreased in all the biochar types, which was likely due to restructuring taking place in the biochar or due to the onset of ash melting at higher temperatures. When comparing the different biochar, Fv offers the highest potential of surface area at 400 ℃ as all other biochar types had a BET specific surface below an average of 50 $m^2 g^{-1}$. The Fv biochar with the highest surface area also had the least ash content while the Le with its highest ash content at 600 ℃ had the least surface area at the same temperature. It has been reported that the higher amount of inorganics (*i.e.,* ash content) in the biochar negatively correlate with specific surface area in the produced biochar (Li and Chen 2018). This is possibly explained by fusion of ash filling up pores in the biochar, thereby decreasing accessible surface area in the other biochar. While the Le biochar had its highest surface area at 600 ℃, the Fv and Tf biochar had their peak values at 400 ℃ and at 500 ℃, respectively. The Le biochar was observed to have relatively smaller surface area compared to the other biochar. Differences in feedstock materials have been suggested as the main reason for the differences in surface area and micropore distribution of biochar (Zhang *et al.* 2018). The majority of pores observed on the biochar samples in this study were mesopores (Table 5 and Figs. 3 to 5). Because the surface areas of Fv biochar ranged from 148.3 $m^2 g^{-1}$ to 210.6 $m^2 g^{-1}$ and was much higher than other samples analyzed (Table 5 and Fig. 1), when added to the soil can improve plant root growth, soil microorganism abundance, soil mineral nutrients, and influence other soil properties (Song *et al.* 2018). Surface area is an important index that they can significantly influence a material's adsorption capacity. A larger surface area resulted in more porous structures within biochar (Windeatt *et al.* 2014), which suggested that Fv biochar may be particularly useful as a soil amendment for water treatment or environmental remediation. Although, further pot and field trials would be required to confirm this.

Fourier Transform Infrared Analysis

The infrared spectra of the biochar revealed the transformation of their complex chemical bond structures at elevated pyrolysis temperatures (Fig. 2). The FTIR peaks appeared between 400 cm^{-1} and 4000 cm^{-1} in all biochar (Fig. 2).

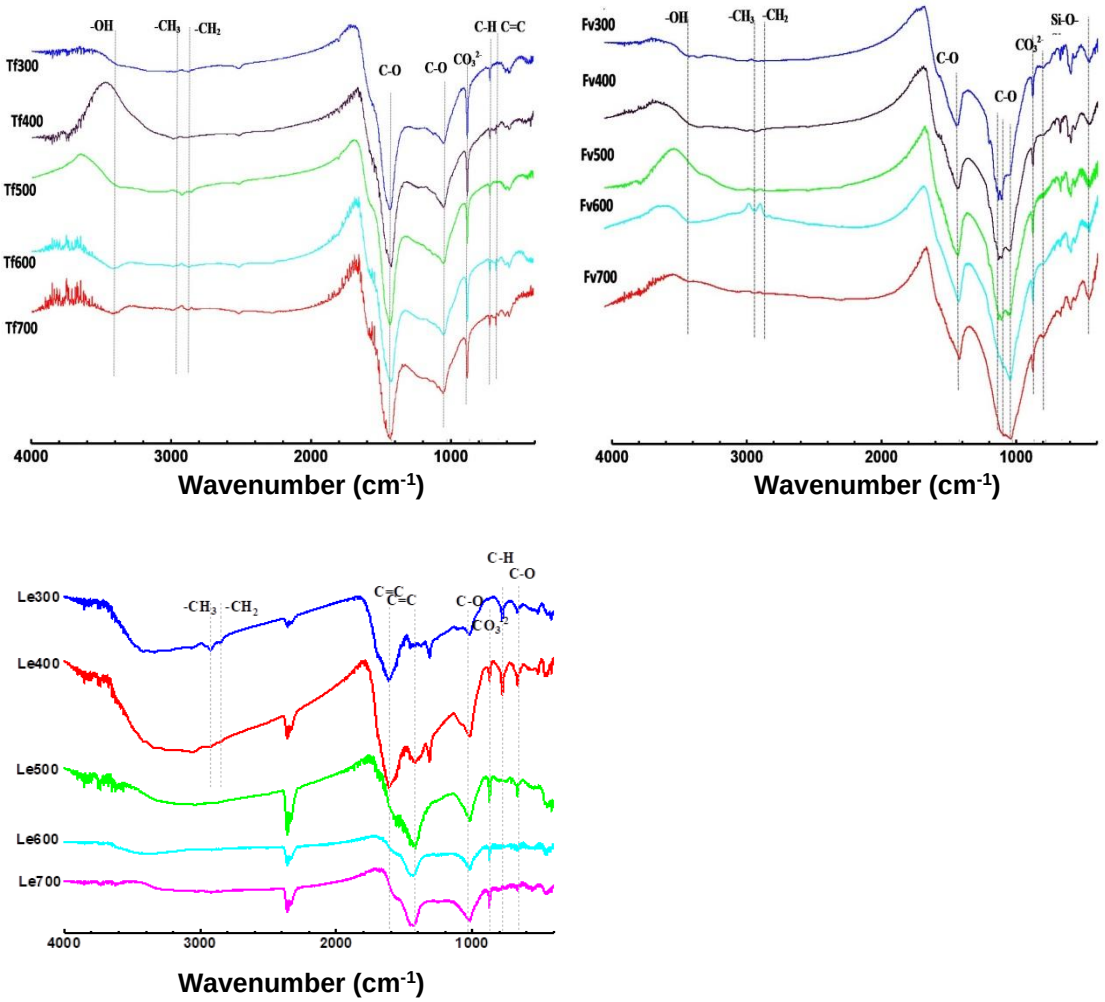

Fig. 2. FTIR spectra of the biochar studied

The disappearance of the -OH group as the pyrolysis temperature increased to 400 °C and above in the Tf and Fv biochar indicated that the organic -OH was very unstable at elevated temperatures. In addition, increasing temperature also had an effect on the functional groups present in the biochar by reducing them, especially the -OH functional groups of phenols, ethers, and alcohol (Sardella *et al.* 2015). Unstable functional groups, such as O-H (near 3400 cm^{-1}), were slightly detected at a high temperature (> 600 °C). In all but Le, the C-O stretching vibration appeared at around 1400 cm^{-1}. Compared to Le, the Fv and Tf biochar exhibited stronger peak intensities for aromatic C-O. Similarly, the -OH groups and C-H groups were weak functional groups, which disappeared for the biochar produced at high pyrolysis temperatures (> 400 °C). The cleavage of -OH and C-H groups contributed to significant mass loss during thermal decomposition and gasification, resulting in decreased biochar yield at high pyrolysis temperatures. Weakening of the peak with the increase in the pyrolysis temperature is often expected (Jin *et al.* 2016). When the pyrolysis temperature was raised to 600 °C, almost no aliphatic functional groups could be found in the biochar. Instead, aliphatic structures were reformed into aromatic structures, resulting in the increased presence of phenolic functional groups and ethers. The C=O stretching vibration in the carboxyl group in the Le biochar appeared at 1400 cm^{-1} and 1600

cm^{-1}. Adsorption peaks that are representatives of different functional groups were observed (Yuan *et al.* 2015; Domingues *et al.* 2017).

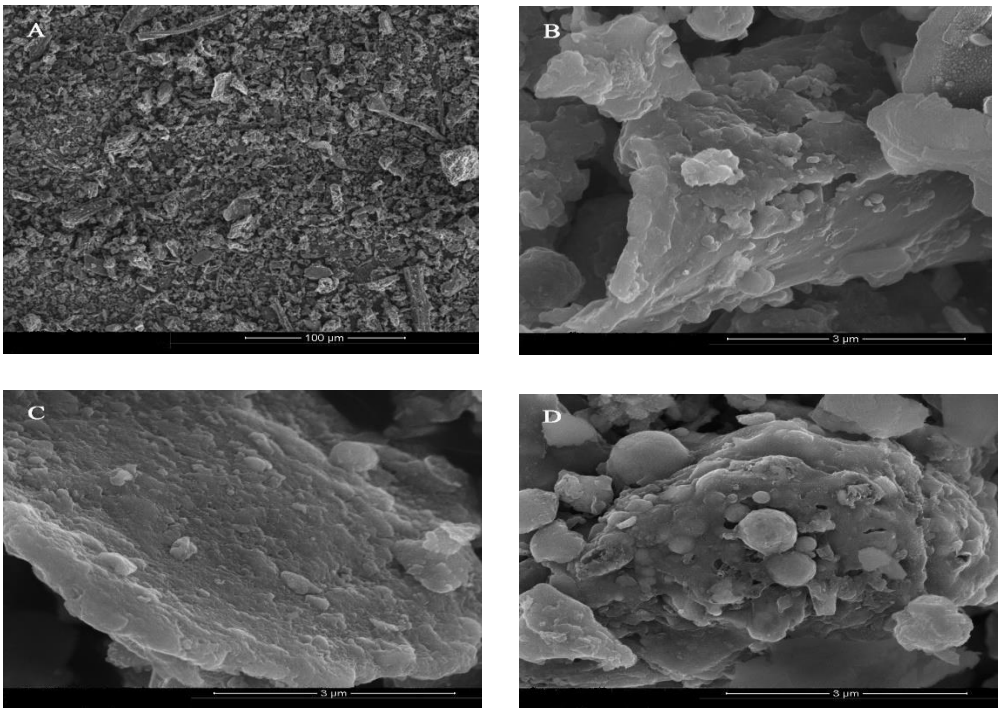

Fig. 3. SEM images of Tf400 biochar at different magnification times

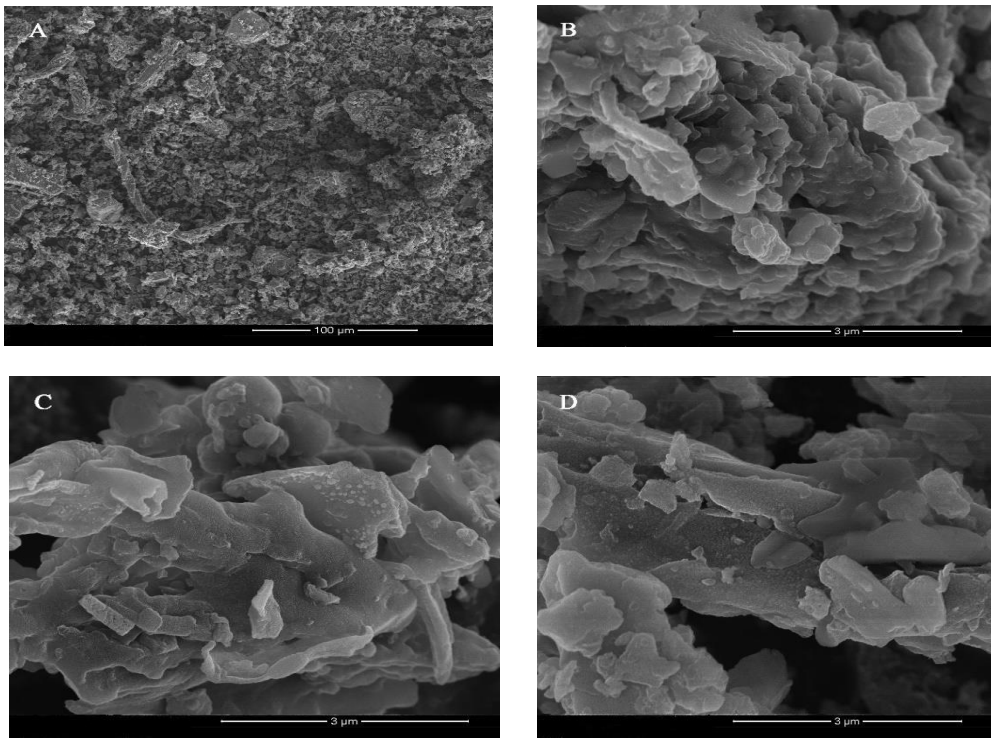

Fig. 4. SEM images of Fv400 biochar at different magnification times

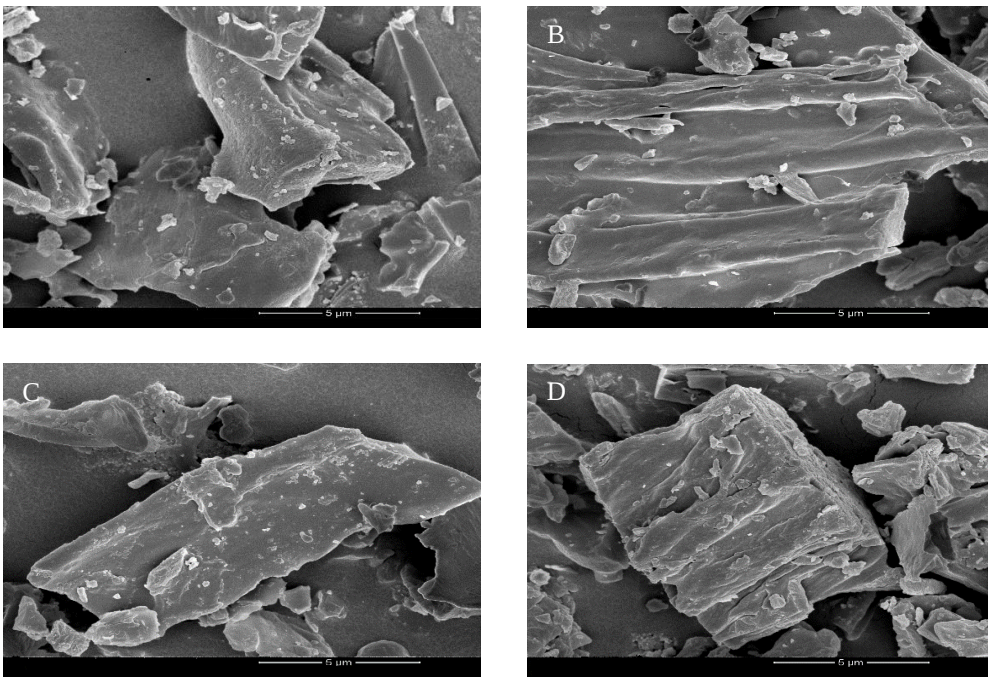

Fig. 5. SEM images of Le400 biochar at different magnification times

The C=C stretching vibrations were identified for biochar (Tf and Le) produced at low temperatures (< 400 °C), but their intensities were weak. Similar observations have been reported (Li and Chen 2018). Although some aromatic C=C structures were reformed, the high pyrolysis temperature of 600 °C or above provided adequate energy to crack many double bonds of C=C, which caused a decrease of C=C structures in the biochar. The CO_3, C-H, and Si-O (in the Fv biochar) stretching and the -CH_2, -CH_3 (slightly detected), and -OH out-of-plane bending vibration of phenols, ethers, and alcohols appeared between 2800 cm^{-1} to 3400 cm^{-1}, while Le had no -OH group. The CO_3 showed strong intensity across all pyrolytic temperatures, showing the high carbon contents in the biochar. This result indicates that samples with different feedstocks will have differential absorption intensities (Zhang *et al*. 2018). Although these biochar have similar functional group types, their concentrations and relative ratios will vary according to the feedstock type and pyrolytic temperature (Dong *et al.* 2014).

X-Ray Diffraction Analysis of Biochar

The XRD patterns among the biochar showed variation in their surface minerals as influenced by the pyrolytic temperatures (Fig. 6). Generally, peaks of SiO_2 and $CaCO_3$ were found on all the biochar samples, though their intensities varied with $CaCO_3$ observed across all temperatures. The presence of $CaCO_3$ was consistent with the high ash contents and alkalinity of the biochar (Fig. 6, Table 3).

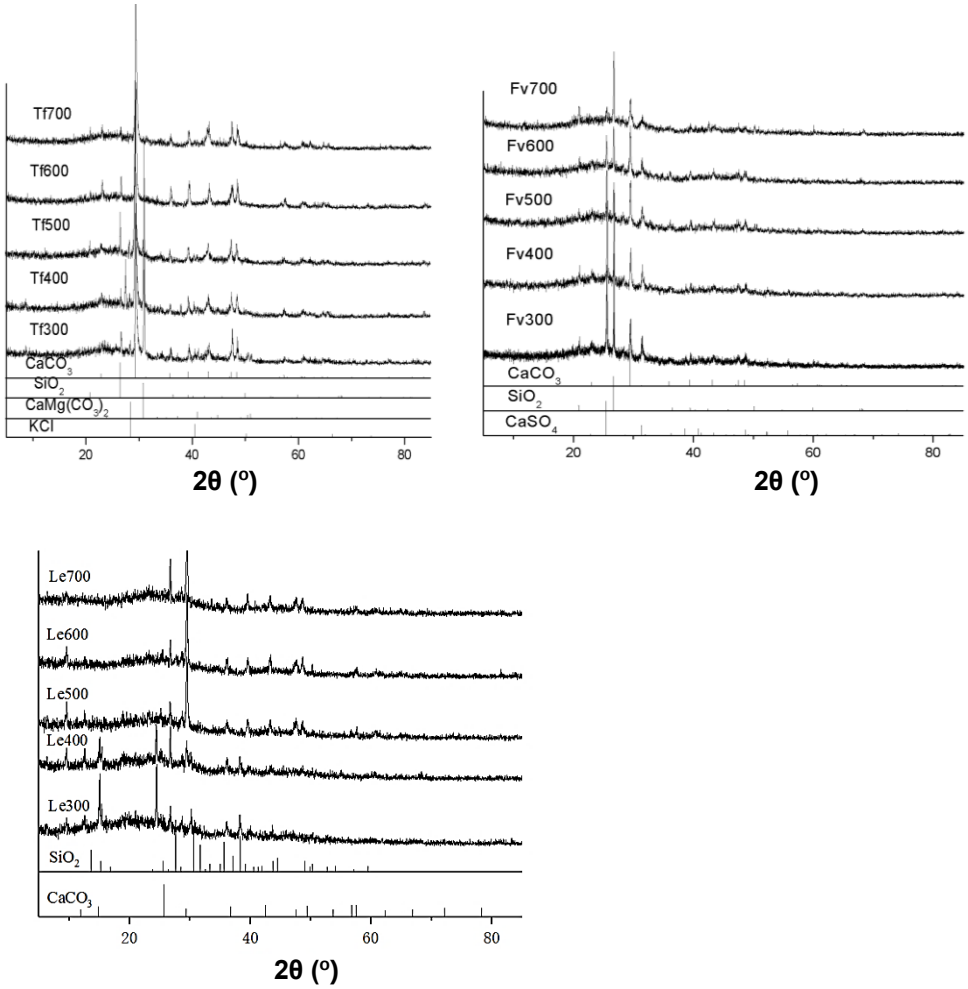

Fig. 6. XRD Analysis of biochar samples at different temperatures

For the Tf biochar, across all temperatures there was a significant characteristic peak of KCl at around the diffraction angle of 30º, which was consistent with the much higher potassium contents measured in the sample (Table 3) and was a signal peak of potassium salt (Kim *et al.* 2012). Other minerals observed on the Tf surface include SiO_2 and $CaMg(CO_3)_2$. The XRD pattern of the Fv biochar had a characteristic peak of $CaSO_4$ (25.5º), consistent with the much higher sulfur contents measured (Table 3). However, the intensity of $CaSO_4$ decreased at the peak temperature of 700 °C. The $CaCO_3$ of the Le biochar reflected the high carbon content, compared to all of the other biochars studied. This also suggested high ash content compared to the other biochar (Zhang *et al.* 2018), which was verified (Table 3). Just like Tf, the Fv biochar had a peak of SiO_2 below 500 °C as well as Le from 500 °C to 700 °C. Figure 5 shows the characteristic peak intensity of SiO_2 decreased as the pyrolysis temperature increased, possibly due to high temperature, which caused the silicon dioxide to react with the carbon and then formed silicon and carbon monoxide. It has been suggested that the concentrations and relative ratios of functional groups in a particular biochar type will vary according to the feedstock type and pyrolytic temperature (Kim *et al.* 2018). Figure 5 shows that the characteristic peak intensity of $CaSO_4$ decreased as the pyrolysis temperature increased, a product of high temperature that caused $CaSO_4$ to oxidize into calcium oxide and sulfur dioxide, which was consistent with the sulfur contents on the overall trend (Table 2).

CONCLUSIONS

1. The yield and volatile matter (VM) of all the biochar tested decreased as the pyrolysis temperature increased with Le300 having the highest yield (47.41%).The highest VM was obtained in Tf300 (79.6%), while Le700 had the least VM (54.1%). The pH values of all the biochar produced were alkaline, and it increased with increasing temperature. Biochar produced at higher pyrolysis temperatures are therefore expected to have more advantages for use as soil amendments on acidic soils (especially the Fv biochar at 700 ^{o}C with the highest pH of 11.6), in contrast to the feedstocks that were acidic.
2. Although all the biochars were relatively high in nutrient composition, highest nutrient contents were observed in the following biochars: Tf300 (N: 2.07 %), Fv700 (P: 11.95 g kg^{-1}), Le700 (K: 21.89 g kg^{-1}), Fv600 (CEC: 32.29 cmol kg^{-1}), Fv700 (Ash: 33.40 %) and Le700 (C: 58.65 %). The high nutrient contents of the biochar obtained suggested that the biochar could be of agronomic use as fertilizers; specific for the nutrients needed using the appropriate biochar stated above if the nutrients were subsequently plant available.
3. The Fv biochar had the highest heavy metal concentrations across all the metals measured. The content of Zn in Fv300 (432.8 mg kg^{-1}) and Ni in Le600 (51.4 mg kg^{-1}) were above the threshold of 400 mg kg^{-1} and 50 mg kg^{-1} respectively, but they can still be used without any environmental concern.
4. The Fv biochars had the largest surface area measured, with Fv400 having the largest surface area (210.6 m^2g^{-1}). This makes it the ideal biochar for adsorption of heavy metals and other organic pollutants in the environment and for improving nutrient retention in soil. Also the Le400 biochar having the highest average pore diameter (159.7 Å) will be ideal for improving the porosity of compacted soils to create and ideal environment for soil organisms.
5. The FTIR spectra showed the presence of various functional groups on the biochar surface with the C-O as dominant (except on the Le biochar). The CO_3 showed strong intensity across all pyrolytic temperatures, confirming the high carbon contents in the biochars (52.6% to 58.6%). The Le biochar had no -OH group unlike the other biochar. This was attributed to the nature of the feedstock. A weakening of peaks of these functional groups with the increase in pyrolysis temperature above 400 °C was observed.
6. The XRD analysis revealed that SiO_2 and $CaCO_3$ were present on all biochar surfaces, with Tf having a characteristic peak of KCl (30^{o}), Fv with a peak of $CaSO_4$ (25.5^{o}), and Le with a peaks indicating high SiO_2 (31^{o}) and $CaCO_3$ (23^{o}).
7. In addition to temperature, the feedstock source and their composition influenced the properties of derived biochar.
8. The results suggested that the produced biochar, depending on their observed properties under the different temperatures, show potential as suitable soil amendments in agronomy and for environmental remediation.

ACKNOWLEDGEMENTS

The authors would like to thank Rongjun Bian for advice and feedback. Funding was provided by the Central Financial Forestry Science and Technology Promotion Demonstration Project (Min[2018]TG15) and the Fujian Science and Technology Major Project (2017NZ0001).

REFERENCES CITED

Ahmad, M., Lee, S. S., Lee, S. E., Al-Wabel, M. I., Tsang, D. C., and Ok, Y. S. (2017). "Biochar-induced changes in soil properties affected immobilization/mobilization of metals/metalloids in contaminated soils," *Journal of Soils and Sediments* 17(3), 717-730. DOI: 10.1007/s11368-015-1339-4

Bais-Moleman, A. L., Sikkema, R., Vis, M., Reumerman, P., Theurl, M. C., and Erb, K.-H. (2018). "Assessing wood use efficiency and greenhouse gas emissions of wood product cascading in the European Union," *Journal of Cleaner Production* 172, 3942-3954. DOI: 10.1016/j.jclepro.2017.04.153

Beiyuan, J., Awad, Y. M., Beckers, F., Tsang, D. C., Ok, Y. S., and Rinklebe, J. (2017). "Mobility and phytoavailability of As and Pb in a contaminated soil using pine sawdust biochar under systematic change of redox conditions," *Chemosphere* 178, 110-118. DOI: 10.1016/j.chemosphere.2017.03.022

Bergeron, S. P., Bradley, R. L., Munson, A., and Parsons, W. (2013). "Physico-chemical and functional characteristics of soil charcoal produced at five different temperatures," *Soil Biology and Biochemistry* 58, 140-146. DOI: 10.1016/j.soilbio.2012.11.017

Bian, R., Li, L., Shi, W., Ma, B., Joseph, S., Li, L., Liu, X., Zheng, J., Zhang, X., Cheng, K., *et al.* (2018). "Pyrolysis of contaminated wheat straw to stabilize toxic metals in biochar but recycle the extract for agricultural use," *Biomass and Bioenergy* 118, 32-39. DOI: 10.1016/j.biombioe.2018.08.003

Bian, R., Ma, B., Zhu, X., Wang, W., Li, L., Joseph, S., Liu, X., and Pan, G. (2016). "Pyrolysis of crop residues in a mobile bench-scale pyrolyser: Product characterization and environmental performance," *Journal of Analytical and Applied Pyrolysis* 119, 52-59. DOI: 10.1016/j.jaap.2016.03.018

Cantrell, K. B., Hunt, P. G., Uchimiya, M., Novak, J. M., and Ro, K. S. (2012). "Impact of pyrolysis temperature and manure source on physicochemical characteristics of biochar," *Bioresource Technology* 107, 419-428. DOI: 10.1016/j.biortech.2011.11.084

Case, S. D., McNamara, N. P., Reay, D. S., Stott, A. W., Grant, H. K., and Whitaker, J. (2015). "Biochar suppresses N_2O emissions while maintaining N availability in a sandy loam soil," *Soil Biology and Biochemistry* 81, 178-185. DOI: 10.1016/j.soilbio.2014.11.012

Cely, P., Gascó, G., Paz-Ferreiro, J., and Méndez, A. (2015). "Agronomic properties of biochars from different manure wastes," *Journal of Analytical and Applied Pyrolysis* 111, 173-182. DOI: 10.1016/j.jaap.2014.11.014

Chen, D., Yu, X., Song, C., Pang, X., Huang, J., and Li, Y. (2016). "Effect of pyrolysis temperature on the chemical oxidation stability of bamboo biochar," *Bioresource Technology* 218, 1303-1306. DOI: 10.1016/j.biortech.2016.07.112

Colantoni, A., Evic, N., Lord, R., Retschitzegger, S., Proto, A., Gallucci, F., and Monarca,

D. (2016). "Characterization of biochars produced from pyrolysis of pelletized agricultural residues," *Renewable and Sustainable Energy Reviews* 64, 187-194. DOI: 10.1016/j.rser.2016.06.003

Domingues, R. R., Trugilho, P. F., Silva, C. A., Melo, I. C. N. A., Melo, L. C. A., Magriotis, Z. M., and Sanchez-Monedero, M. A. (2017). "Properties of biochar derived from wood and high-nutrient biomasses with the aim of agronomic and environmental benefits," *PLOS One* 12(5), e0176884. DOI: 10.1371/journal.pone.0176884

Dong, X., Ma, L. Q., Gress, J., Harris, W., and Li, Y. (2014). "Enhanced Cr (VI) reduction and As (III) oxidation in ice phase: Important role of dissolved organic matter from biochar," *Journal of Hazardous Materials* 267, 62-70. DOI: 10.1016/j.jhazmat.2013.12.027

Dunnigan, L., Morton, B. J., Hall, P. A., and Kwong, C. W. (2018). "Production of biochar and bioenergy from rice husk: Influence of feedstock drying on particulate matter and the associated polycyclic aromatic hydrocarbon emissions," *Atmospheric Environment* 190, 218-225. DOI: 10.1016/j.atmosenv.2018.07.028

European Biochar Certificate (EBC) (2017). *European Biochar Certificate - Guideline of the European Biochar Certificate* (Version 6.3), European Biochar Foundation, Arbaz, Switzerland. DOI: 10.13140/RG.2.1.4658.7043

Egamberdieva, D., Hua, M., Reckling, M., Wirth, S., and Bellingrath-Kimura, S. D. (2018). "Potential effects of biochar-based microbial inoculants in agriculture," *Environmental Sustainability* 1(1), 19-24. DOI: 10.1007/s42398-018-0010-6

Egamberdieva, D., Reckling, M., and Wirth, S. (2017). "Biochar-based Bradyrhizobium inoculum improves growth of lupin (*Lupinus angustifolius* L.) under drought stress," *European Journal of Soil Biology* 78, 38-42. DOI: 10.1016/j.ejsobi.2016.11.007

Gai, X., Wang, H., Liu, J., Zhai, L., Liu, S., Ren, T., and Liu, H. (2014). "Effects of feedstock and pyrolysis temperature on biochar adsorption of ammonium and nitrate," *PLoS ONE* 9(12), e113888. DOI: 10.1371/journal.pone.0113888

Gascó, G., Paz-Ferreiro, J., Álvarez, M., Saa, A., and Méndez, A. (2018). "Biochars and hydrochars prepared by pyrolysis and hydrothermal carbonisation of pig manure," *Waste Management* 79, 395-403. DOI: 10.1016/j.wasman.2018.08.015

Gaskin, J. W., Speir, R. A., Harris, K., Das, K. C., Lee, R. D., Morris, L. A., and Fisher, D. S. (2010). "Effect of peanut hull and pine chip biochar on soil nutrients, corn nutrient status, and yield," *Agronomy Journal* 102(2), 623. DOI: 10.2134/agronj2009.0083

Ghanim, B. M., Pandey, D. S., Kwapinski, W., and Leahy, J. J. (2016). "Hydrothermal carbonisation of poultry litter: Effects of treatment temperature and residence time on yields and chemical properties of hydrochars," *Bioresource Technology* 216, 373-380. DOI: 10.1016/j.biortech.2016.05.087

Han, L., Ro, K. S., Sun, K., Sun, H., Wang, Z., Libra, J. A., and Xing, B. (2016). "New evidence for high sorption capacity of hydrochar for hydrophobic organic pollutants," *Environmental Science and Technology* 50(24), 13274-13282. DOI: 10.1021/acs.est.6b02401

Han, Y., Boateng, A. A., Qi, P. X., Lima, I. M., and Chang, J. (2013). "Heavy metal and phenol adsorptive properties of biochars from pyrolyzed switchgrass and woody biomass in correlation with surface properties," *Journal of Environmental Management* 118, 196-204. DOI: 10.1016/j.jenvman.2013.01.001

Herath, H., Camps-Arbestain, M., Hedley, M., Kirschbaum, M., Wang, T., and Van Hale,

R. (2015). "Experimental evidence for sequestering C with biochar by avoidance of CO_2 emissions from original feedstock and protection of native soil organic matter," *GCB Bioenergy* 7(3), 512-526. DOI: 10.1111/gcbb.12183

Hmid, A., Mondelli, D., Fiore, S., Fanizzi, F. P., Al Chami, Z., and Dumontet, S. (2014). "Production and characterization of biochar from three-phase olive mill waste through slow pyrolysis," *Biomass and Bioenergy* 71, 330-339. DOI: 10.1016/j.biombioe.2014.09.024

Hossain, M. M., Scott, I. M., McGarvey, B. D., Conn, K., Ferrante, L., Berruti, F., and Briens, C. (2013). "Toxicity of lignin, cellulose and hemicellulose-pyrolyzed bio-oil combinations: Estimating pesticide resources," *Journal of Analytical and Applied Pyrolysis* 99, 211-216. DOI: 10.1016/j.jaap.2012.07.008

Jaafar, N. M., Clode, P. L., and Abbott, L. K. (2015). "Soil microbial responses to biochars varying in particle size surface and pore properties," *Pedosphere* 25,770-778. DOI: 10.1016/S1002-0160(15)30058-8

Jin, J., Li, Y., Zhang, J., Wu, S., Cao, Y., Liang, P., Zhang, J., Wong, M. H., Wang, M., Shan, S., *et al.* (2016). "Influence of pyrolysis temperature on properties and environmental safety of heavy metals in biochars derived from municipal sewage sludge," *Journal of Hazardous Materials* 320, 417-426. DOI: 10.1016/j.jhazmat.2016.08.050

Jindo, K., Mizumoto, H., Sawada, Y., Sanchez-Monedero, M. A., and Sonoki, T. (2014). "Physical and chemical characterization of biochars derived from different agricultural residues," *Biogeosciences* 11(23), 6613-6621. DOI: 10.5194/bg-11-6613-2014

Jouiad, M., Al-Nofeli, N., Khalifa, N., Benyettou, F., and Yousef, L. F. (2015). "Characteristics of slow pyrolysis biochars produced from rhodes grass and fronds of edible date palm," *Journal of Analytical and Applied Pyrolysis* 111, 183-190. DOI: 10.1016/j.jaap.2014.10.024

Kang, S.-W., Kim, S.-H., Park, J.-H., Seo, D.-C., Ok, Y. S., and Cho, J.-S. (2018). "Effect of biochar derived from barley straw on soil physicochemical properties, crop growth, and nitrous oxide emission in an upland field in South Korea," *Environmental Science and Pollution Research* 25(26), 25813-25821. DOI: 10.1007/s11356-018-1888-3

Kerré, B., Willaert, B., Cornelis, Y., and Smolders, E. (2017). "Long-term presence of charcoal increases maize yield in Belgium due to increased soil water availability," *European Journal of Agronomy* 91, 10-15. DOI: 10.1016/j.eja.2017.09.003

Kim, H.-B., Kim, S.-H., Jeon, E.-K., Kim, D.-H., Tsang, D. C., Alessi, D. S., Kwon, E. E., and Baek, K. (2018). "Effect of dissolved organic carbon from sludge, rice straw and spent coffee ground biochar on the mobility of arsenic in soil," *Science of The Total Environment* 636, 1241-1248. DOI: 10.1016/j.scitotenv.2018.04.406

Kim, K. H., Kim, J.-Y., Cho, T.-S., and Choi, J. W. (2012). "Influence of pyrolysis temperature on physicochemical properties of biochar obtained from the fast pyrolysis of pitch pine (*Pinus rigida*)," *Bioresource Technology* 118, 158-162. DOI: 10.1016/j.biortech.2012.04.094

Kung, C.-C., Kong, F., and Choi, Y. (2015). "Pyrolysis and biochar potential using crop residues and agricultural wastes in China," *Ecological Indicators* 51, 139-145. DOI: 10.1016/j.ecolind.2014.06.043

Lehmann, J., Rillig, M. C., Thies, J., Masiello, C. A., Hockaday, W. C., and Crowley, D. (2011). "Biochar effects on soil biota – A review," *Soil Biology and Biochemistry* 43, 1812-1836. DOI: 10.1016/j.soilbio.2011.04.022

Li, S., Barreto, V., Li, R., Chen, G., and Hsieh, Y. P. (2018). "Nitrogen retention of biochar derived from different feedstocks at variable pyrolysis temperatures," *Journal of Analytical and Applied Pyrolysis* 133, 136-146. DOI: 10.1016/j.jaap.2018.04.010

Li, S., and Chen, G. (2018). "Thermogravimetric, thermochemical, and infrared spectral characterization of feedstocks and biochar derived at different pyrolysis temperatures," *Waste Management* 78, 198-207. DOI: 10.1016/j.wasman.2018.05.048

Li, Y., Meas, A., Shan, S., Yang, R., and Gai, X. (2016). "Production and optimization of bamboo hydrochars for adsorption of Congo red and 2-naphthol," *Bioresource Technology* 207, 379-386. DOI: 10.1016/j.biortech.2016.02.012

Lim, S.-H., Lee, Y.-H., and Kang, H.-W. (2013). "Efficient recovery of lignocellulolytic enzymes of spent mushroom compost from Oyster mushrooms, *Pleurotus spp*., and potential use in dye decolorization," *Mycobiology* 41(4), 214-220. DOI: 10.5941/MYCO.2013.41.4.214

Mao, Y., Heiling, M., Zou, S., Xing, S., Zhao, Z., and Huang, Z. (2018). "Effects of biochar from spent mushroom substrate on the physicochmical properties in a nutrient-poor soil," in: *20th EGU General Assembly*, Vienna, Austria, pp. 3961.

Mechler, M., Jiang, R., Silverthorn, T., and Oelbermann, M. (2018). "Impact of biochar on soil characteristics and temporal greenhouse gas emissions: A field study from southern Canada," *Biomass and Bioenergy* 118, 154-162. DOI: 10.1016/j.biombioe.2018.08.019

Molnar, M., Vaszita, E., Farkas, E., Ujaczki, E., Fekete-Kertesz, I., Tolner, M., Klebercz, O., Kirchkeszner, C., Gruiz, K., Uzinger, N., *et al.* (2016). "Acidic sandy soil improvement with biochar - A microcosm study," *Science of The Total Environment* 563-564, 855-865. DOI: 10.1016/j.scitotenv.2016.01.091

Mukherjee, A., Zimmerman, A.R., and Harris, W. (2011). "Surface chemistry variations among a series of laboratory-produced biochars," *Geoderma* 163, 247-255. DOI: 10.1016/j.geoderma.2011.04.021

Nanda, S., Azargohar, R., Kozinski, J. A., and Dalai, A. K. (2014). "Characteristic studies on thepyrolysis products from hydrolyzed canadian lignocellulosic feedstocks," *Bioenergy Research* 7(1), 174-191. DOI: 10.1007/s12155-013-9359-7

Paula, F. S., Tatti, E., Abram, F., Wilson, J., and O'Flaherty, V. (2017). "Stabilisation of spent mushroom substrate for application as a plant growth-promoting organic amendment," *Journal of Environmental Management* 196, 476-486. DOI: 10.1016/j.jenvman.2017.03.038

Peng, X., Ye, L., Wang, C., Zhou, H., and Sun, B. (2011). "Temperature-and duration-dependent rice straw-derived biochar: Characteristics and its effects on soil properties of an Ultisol in southern China," *Soil and Tillage Research* 112(2), 159-166. DOI: 10.1016/j.still.2011.01.002

Phan, C.-W., and Sabaratnam, V. (2012). "Potential uses of spent mushroom substrate and its associated lignocellulosic enzymes," *Applied Microbiology and Biotechnology* 96(4), 863-873. DOI: 10.1007/s00253-012-4446-9

Ronsse, F., Hecke, S. V., Dickinson, D., and Prins, W. (2013). "Production and characterization of slow pyrolysis biochar: Influence of feedstock type and pyrolysis conditions," *GCB Bioenergy - Special Issue: Biochar* 5(2), 104-115. DOI: 10.1111/gcbb.12018

Sardella, F., Gimenez, M., Navas, C., Morandi, C., Deiana, C., and Sapag, K. (2015). "Conversion of viticultural industry wastes into activated carbons for removal of lead and cadmium," *Journal of Environmental Chemical Engineering* 3(1), 253-260. DOI:

10.1016/j.jece.2014.06.026

Song, D., Tang, J., Xi, X., Zhang, S., Liang, G., Zhou, W., and Wang, X. (2018). "Responses of soil nutrients and microbial activities to additions of maize straw biochar and chemical fertilization in a calcareous soil," *European Journal of Soil Biology* 84, 1-10. DOI: 10.1016/j.ejsobi.2017.11.003

Subedi, R., Taupe, N., Ikoyi, I., Bertora, C., Zavattaro, L., Schmalenberger, A., Leahy, J., and Grignani, C. (2016). "Chemically and biologically-mediated fertilizing value of manure-derived biochar," *Science of The Total Environment* 550, 924-933. DOI: 10.1016/j.scitotenv.2016.01.160

Sun, Y., Gao, B., Yao, Y., Fang, J., Zhang, M., Zhou, Y., Chen, H., and Yang, L. (2014). "Effects of feedstock type, production method, and pyrolysis temperature on biochar and hydrochar properties," *Chemical Engineering Journal* 240, 574-578. DOI: 10.1016/j.cej.2013.10.081

Vecstaudza, D., Grantina-Ievina, L., Makarenkova, G., Kasparinskis, R., Selga, T., Steinberga, V., Stelmahere, S., Steiner, C., and Muter, O. (2018). "The impact of wood-derived biochar on the survival of *Trichoderma spp*. and growth of *Secale cereale* L. in sandy soil," *Biocontrol Science and Technology* 28(4), 341-358. DOI: 10.1080/09583157.2018.1450488

Wang, H., Wang, X., Cui, Y., Xue, Z., and Ba, Y. (2018). "Slow pyrolysis polygeneration of bamboo (*Phyllostachys pubescens*): Product yield prediction and biochar formation mechanism," *Bioresource Technology* 263, 444-449. DOI: 10.1016/j.biortech.2018.05.040

Wang, H., Xia, W., and Lu, P. (2017). "Study on adsorption characteristics of biochar on heavy metals in soil," *Korean Journal of Chemical Engineering* 34(6), 1867-1873. DOI: 10.1007/s11814-017-0048-7

Wang, Y., Lin, Y., Chiu, P. C., Imhoff, P. T., and Guo, M. (2015). "Phosphorus release behaviors of poultry litter biochar as a soil amendment," *Science of The Total Environment* 512-513, 454-463. DOI: 10.1016/j.scitotenv.2015.01.093

Wang, Y., Yin, R., and Liu, R. (2014). "Characterization of biochar from fast pyrolysis and its effect on chemical properties of the tea garden,"*Journal of Analytical and Applied Pyrolysis* 110, 375-381. DOI: 10.1016/j.jaap.2014.10.006

Wang, Z., Han, L., Sun, K., Jin, J., Ro, K. S., Libra, J. A., Liu, X., and Xing, B. (2016). "Sorption of four hydrophobic organic contaminants by biochars derived from maize straw, wood dust and swine manure at different pyrolytic temperatures," *Chemosphere* 144, 285-291. DOI: 10.1016/j.chemosphere.2015.08.042

Weber, K., and Quicker, P. (2018). "Properties of biochar," *Fuel* 217, 240-261. DOI: 10.1016/j.fuel.2017.12.054

Windeatt, J. H., Ross, A. B., Williams, P. T., Forster, P. M., Nahil, M. A., and Singh, S. (2014). "Characteristics of biochars from crop residues: Potential for carbon sequestration and soil amendment," *Journal of Environmental Management* 146, 189-197. DOI: 10.1016/j.jenvman.2014.08.003

Xiao, R., Wang, J. J., Gaston, L. A., Zhou, B., Park, J.-H., Li, R., Dodla, S. K., and Zhang, Z. (2018). "Biochar produced from mineral salt-impregnated chicken manure: Fertility properties and potential for carbon sequestration," *Waste Management* 78, 802-810. DOI: 10.1016/j.wasman.2018.06.047

Yadav, P., and Samadder, S. (2018). "A critical review of the life cycle assessment studies on solid waste management in Asian countries," *Journal of Cleaner Production* 185, 492-515. DOI: 10.1016/j.jclepro.2018.02.298

Yargicoglu, E. N., Sadasivam, B. Y., Reddy, K. R., and Spokas, K. (2015). "Physical and chemical characterization of waste wood derived biochars," *Waste Management* 36, 256-268. DOI: 10.1016/j.wasman.2014.10.029

Yoo, J.-C., Beiyuan, J., Wang, L., Tsang, D. C., Baek, K., Bolan, N. S., Ok, Y. S., and Li, X.-D. (2018). "A combination of ferric nitrate/EDDS-enhanced washing and sludge-derived biochar stabilization of metal-contaminated soils," *Science of The Total Environment* 616-617, 572-582. DOI: 10.1016/j.scitotenv.2017.10.310

Yuan, H., Lu, T., Huang, H., Zhao, D., Kobayashi, N., and Chen, Y. (2015). "Influence of pyrolysis temperature on physical and chemical properties of biochar made from sewage sludge," *Journal of Analytical and Applied Pyrolysis* 112, 284-289. DOI: 10.1016/j.jaap.2015.01.010

Zhang, C., He, C., and Qiao, Y. (2018). "Lower-temperature pyrolysis to prepare biochar from agricultural wastes and adsorption for Pb^{2+}," *BioResources* 13(3), 5543-5553. DOI: 10.15376/biores.13.3.5543-5553

Zhang, J., Liu, J., and Liu, R. (2015). "Effects of pyrolysis temperature and heating time on biochar obtained from the pyrolysis of straw and lignosulfonate," *Bioresource Technology* 176, 288-291. DOI: 10.1016/j.biortech.2014.11.011

Zhou, X., Qiao, M., Su, J.-Q., Wang, Y., Cao, Z.-H., Cheng, W.-D., and Zhu, Y.-G. (2019). "Turning pig manure into biochar can effectively mitigate antibiotic resistance genes as organic fertilizer," *Science of The Total Environment* 649, 902-908. DOI: 10.1016/j.scitotenv.2018.08.368

Article submitted: March 18, 2019; Peer review completed: April 20, 2019; Revised version received and accepted: May 9, 2019; Published: May 13, 2019.
DOI: 10.15376/biores.14.3.5254-5277